

ELECTRONIC SUPPLEMENTARY INFORMATION (ESI)

Tailored activated carbons for supercapacitors derived from hydrothermally carbonized sugars by chemical activation

Kian Keat Lee^a, Wenming Hao^a, Mikaela Gustafsson^a, Cheuk-Wai Tai^a, Daniel Morin^b, Eva Björkman^c, Malte Lilliestråle^c, Fredrik Björefors^d, Anna M. Andersson^{b,*}, Niklas Hedin^{a,*}

^aDepartment of Materials and Environmental Chemistry-Arrhenius Laboratory, Stockholm University, SE-106 91 Stockholm, Sweden.

^bABB Corporate Research, Forskargränd 7, SE-721 78 Västerås, Sweden.

^cBiokol Lilliestråle & Co KB, Sibyllegatan 53, SE-114 43 Stockholm, Sweden.

^dDepartment of Chemistry-Ångström Laboratory, Uppsala University, Box 538, SE-751 21 Uppsala, Sweden.

*anna.m.andersson@se.abb.com (A.M. Andersson), *niklas.hedin@mmk.su.se (N. Hedin)

CONTENTS

No.	Caption	Page
Table S1	Comparison of specific capacitance (C_m) values calculated from voltage ranges of 0 to 1 V, 0 to 0.9 V and 0 to 0.8 V.	3
Figure S1	Test set-up for measuring electrical conductivity of AC powders.	4
Figure S2	Thermogravimetric analysis (TGA) showed that HTC-GA is more difficult to combust compared to HTC-G.	4
Figure S3	N_2 adsorption-desorption isotherms at -196 °C for AC-GFe-800-2h and AC-GFe-800-4h. Filled and empty symbols represent adsorption and desorption, respectively.	5
Figure S4	XPS wide spectra of AC-G-700 (a), AC-GFe-700 (b) and AC-GFe-800-2h (c).	6
Figure S5	XPS wide spectra of AC-GA-700 (a), AC-GA-800 (b) and AC-GAFe-700 (c).	7
Figure S6	High-resolved C 1s spectra of AC-G-700 (a), AC-GFe-700 (b) and AC-GFe-800-2h (c).	8
Figure S7	High-resolved C 1s spectra of AC-GA-700 (a), AC-GA-800 (b) and AC-GAFe-700 (c).	9
Figure S8	Relationship between the activation temperature and bulk elemental composition for different series of ACs.	10
Figure S9	XRD patterns of different ACs	11
Figure S10	Galvanostatic charge-discharge curves of different AC series at 0.2 A/g.	12
Figure S11	CV curves of sample AC-G-700 at different scan rates from 2 to 200 mV/s.	13
Figure S12	Galvanostatic charge-discharge curves of AC-G series and corresponding specific capacitances (C_m).	13
Figure S13	Effects of activation temperatures and precursor types on electrical conductivity of AC powders.	14
Figure S14	Cycling life time of AC-G-700 in 6 M KOH.	14
Figure S15	Raman spectra of AC samples	15
Figure S16	(a) SEM, (b) TEM, (c, d) HRTEM, (e) BF-STEM and (f) HAADF-STEM images of AC-G-700.	17
Figure S17	EELS spectra in the carbon K-edge region from the sample AC-G-700 and amorphous carbon.	18

Table S1. Comparison of specific capacitance (C_m) values calculated from voltage ranges (E) of 0 to 1 V, 0 to 0.9 V and 0 to 0.8 V based on CV curves at 2 mV/s and galvanostatic discharge curves (CP) at 0.2 A/g.

ACs	C_m (F/g) E: 0 to 1 V		C_m (F/g) E: 0 to 0.90 V		C_m (F/g) E: 0 to 0.80 V	
	CV	CP	CV	CP	CV	CP
AC-GFe-600	203	193	206	202	211	210
AC-GFe-700	241	232	240	240	245	250
AC-GFe-750	246	234	245	242	247	251
AC-GFe-800-2h	255	240	256	246	257	253
AC-GFe-800	217	208	218	216	219	224
AC-G-600	233	227	238	238	247	253
AC-G-700	258	247	260	251	264	259
AC-G-800	215	204	217	210	219	216
AC-GAFe-600	243	233	254	248	269	265
AC-GAFe-700	251	242	254	250	259	261
AC-GAFe-800	230	226	232	234	236	243
AC-GA-600	215	203	225	216	237	231
AC-GA-700	263	250	268	255	276	269
AC-GA-800	226	214	225	226	231	238
Norit SX Ultra	92	84	93	86	94	88

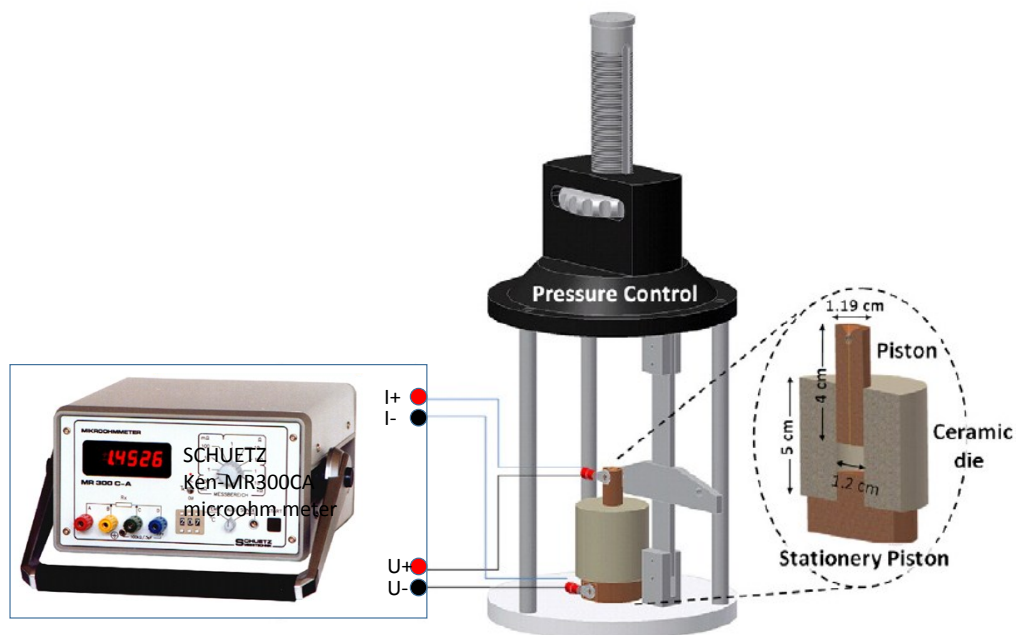


Figure S1. Test set-up for measuring electrical conductivity of AC powders.

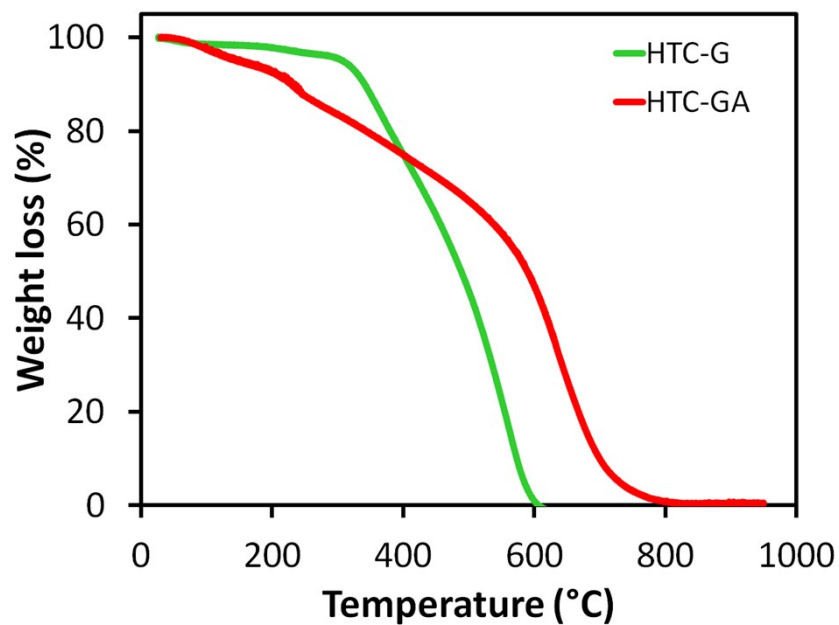


Figure S2. Thermogravimetric analysis (TGA) showed that HTC-GA is more difficult to combust compared to HTC-G.

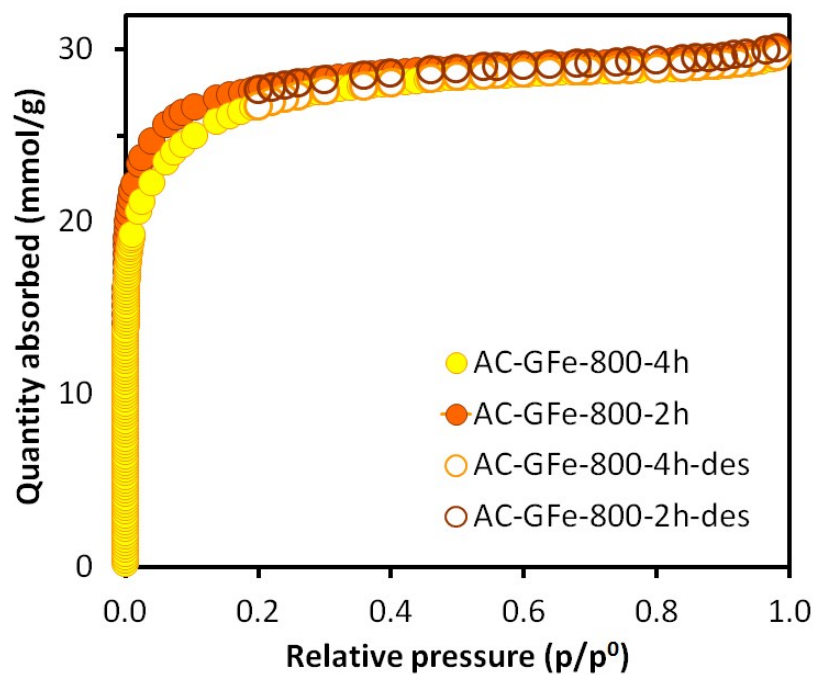


Figure S3. N₂ adsorption-desorption isotherms at -196 °C for AC-GFe-800-2h and AC-GFe-800-4h. Filled and empty symbols represent adsorption and desorption, respectively. Activated carbons (AC-X-Y) from hydrothermally carbonized glucose with iron (X: GFe) prepared at a temperature of Y: 800 °C for 2 or 4 h.

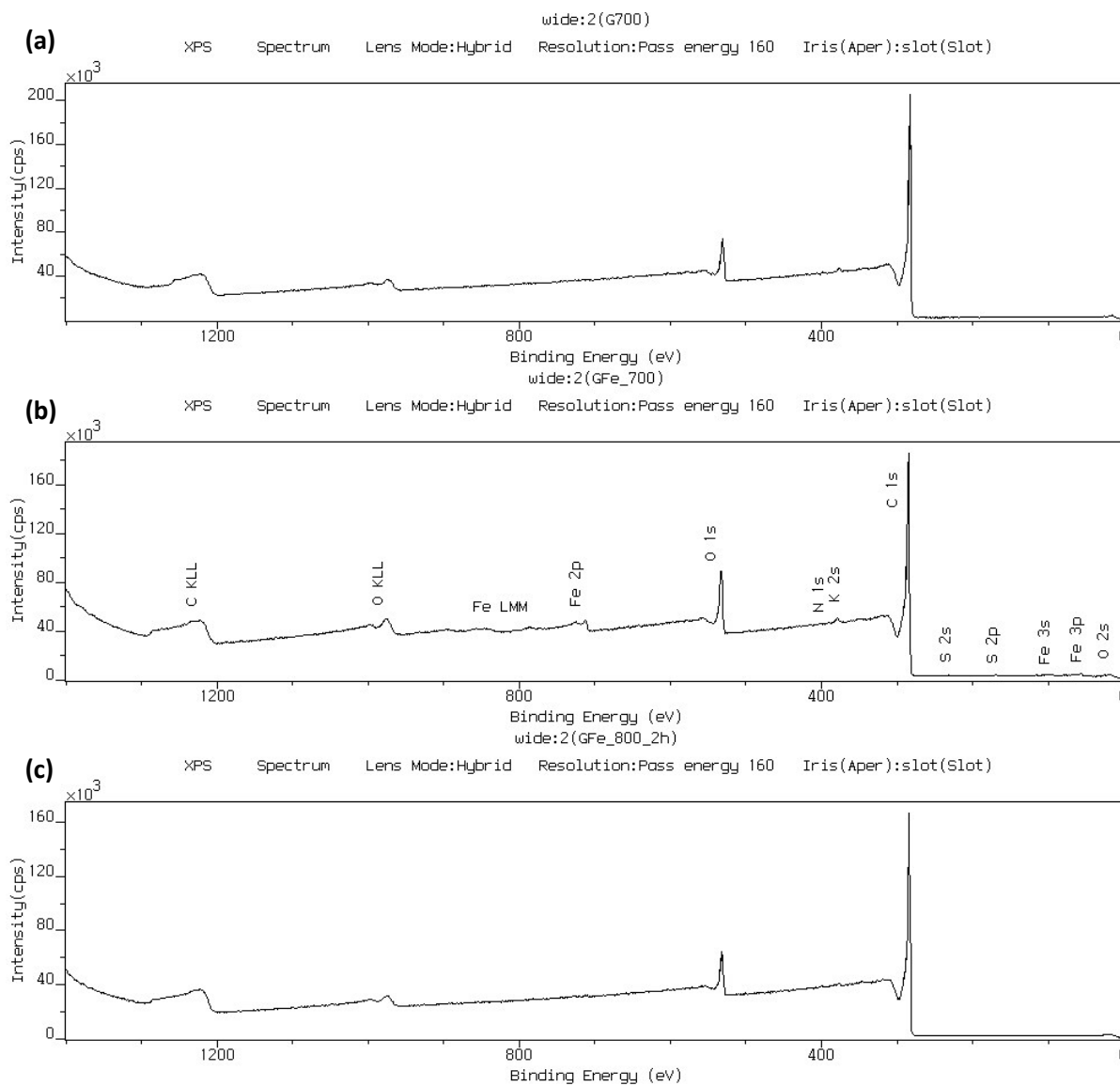


Figure S4. XPS wide spectra of AC-G-700 (a), AC-GFe-700 (b) and AC-GFe-800-2h (c).

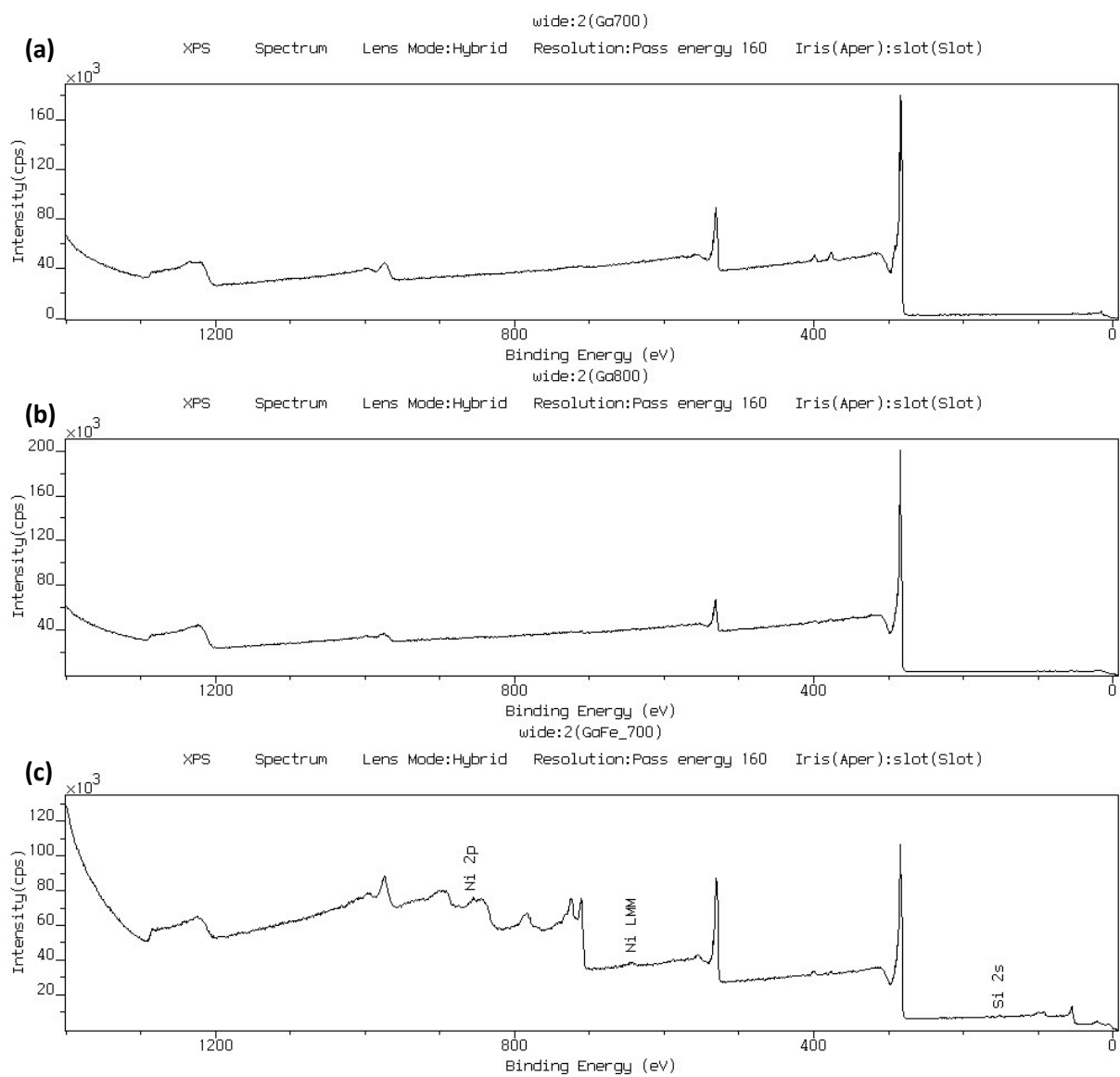


Figure S5. XPS wide spectra of AC-GA-700 (a), AC-GA-800 (b) and AC-GAFe-700 (c).

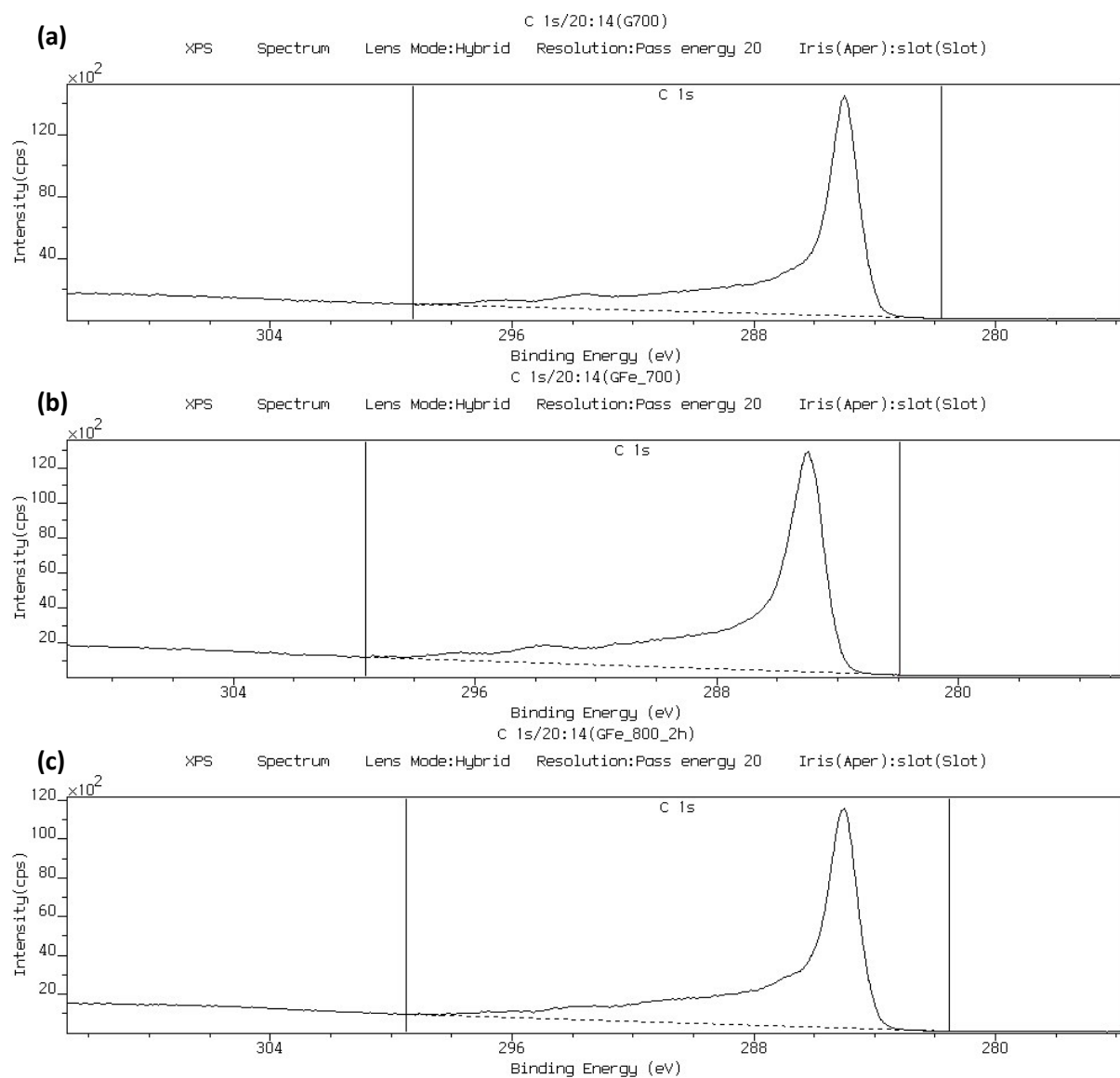


Figure S6. High-resolved C 1s spectra of AC-G-700 (a), AC-GFe-700 (b) and AC-GFe-800-2h (c).

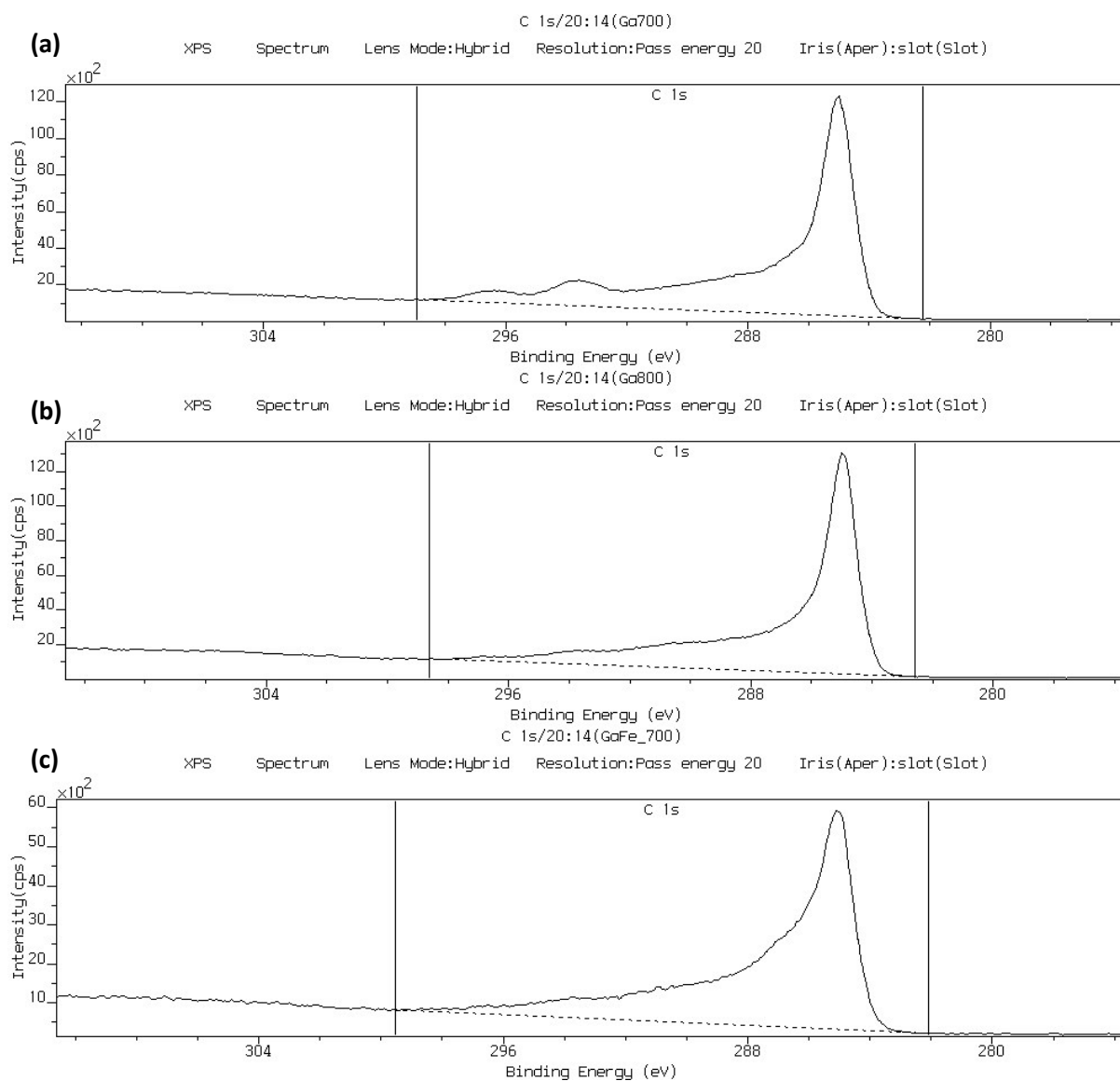


Figure S7. High-resolved C 1s spectra of AC-GA-700 (a), AC-GA-800 (b) and AC-GAFc-700 (c).

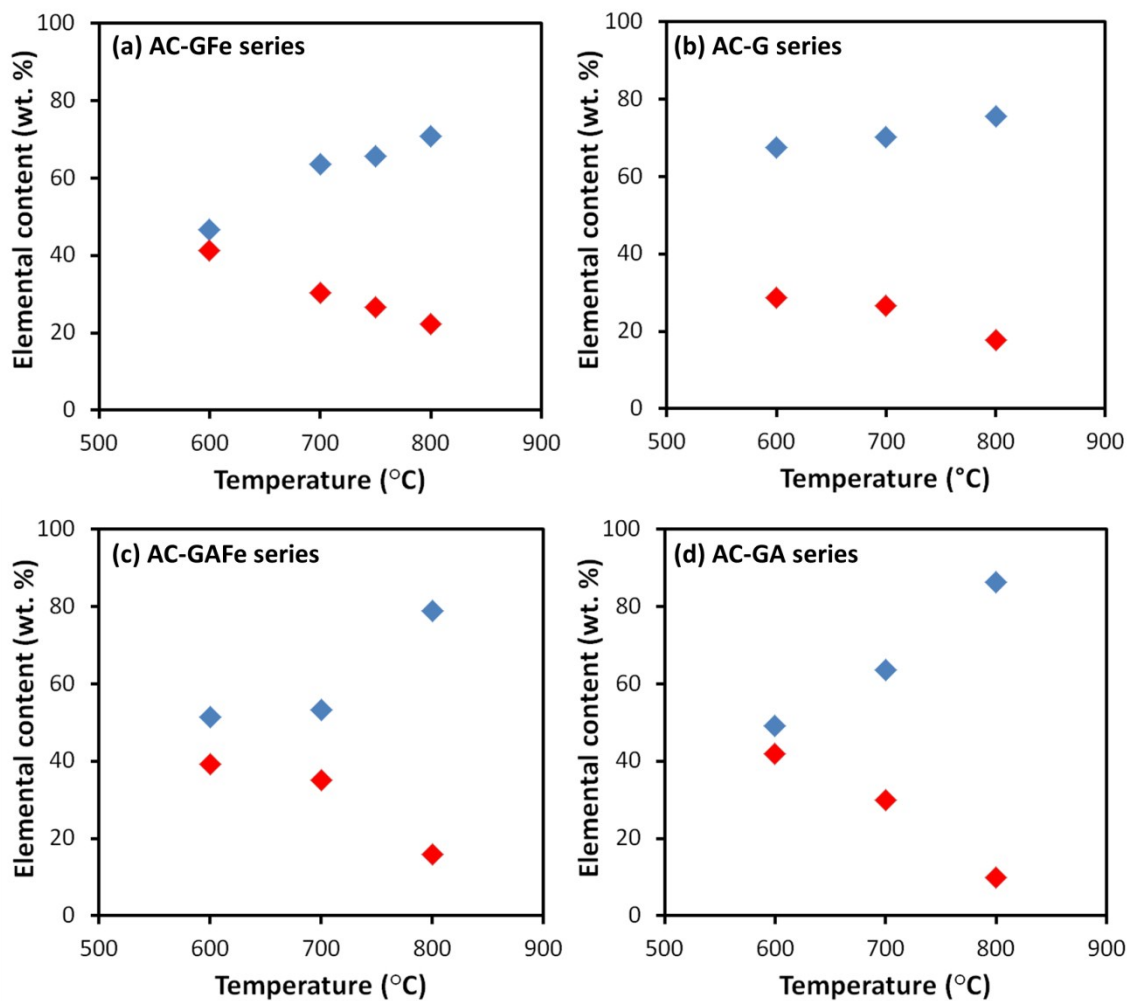


Figure S8. Relationship between the activation temperature and bulk elemental composition (*blue diamond*: carbon content; *red diamond*: oxygen content) for different series of ACs. Oxygen content was calculated by difference.

Concerning the type of iron species, XRD was applied to assess the phases as shown in Figure 6. For the AC-G with low Fe contaminants (AC-G-600 and 700), a typical XRD pattern as in Figure 6a was recorded. Two broad humps roughly centered at 20° and 43° 2Theta corresponding to amorphous carbon with microcrystalline domains. For AC-G-800 with 4.39 wt. % Fe, distinct peaks were observed. The XRD peaks can be matched to metallic iron phases [Fe (04-014-0264) and Fe (04-004-2475)] which account to > 90 % of iron species based on semi-quantitative analysis by Panalytical HighScore Plus software. The rest of iron species may be related to Fe₃O₄ and FeO, but it is not conclusive due to the low signals.

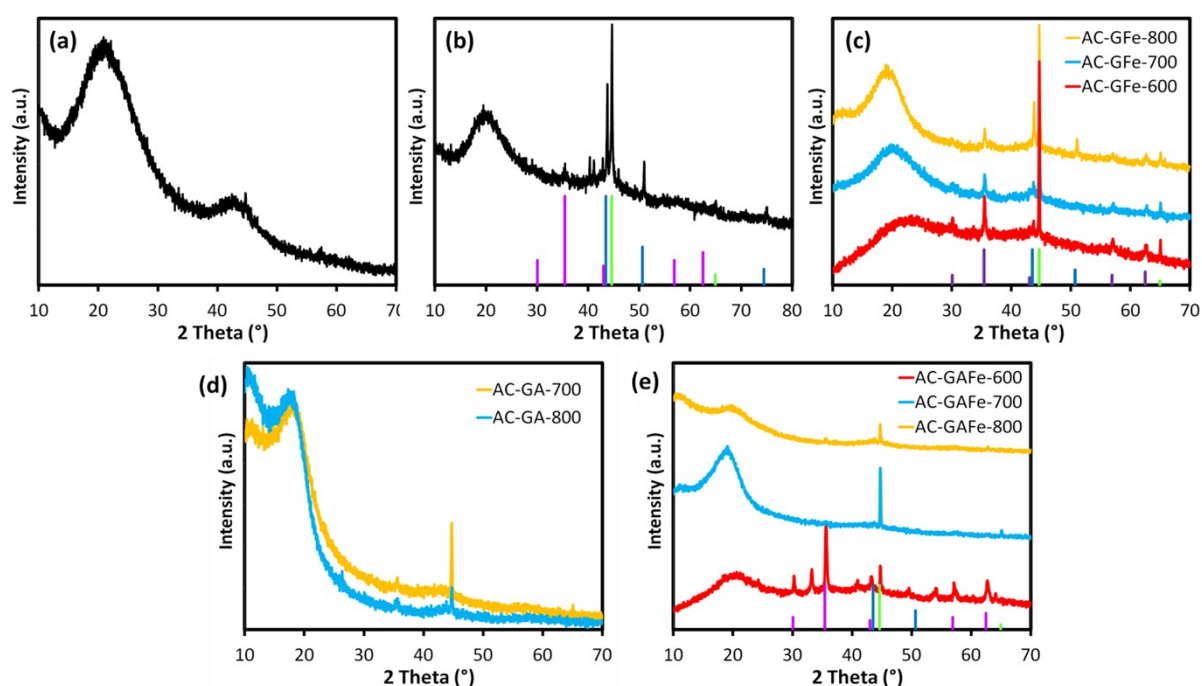


Figure S9. XRD patterns of different ACs: (a) AC-G-600, (b) AC-G-800, (c) AC-GFe series, (d) AC-GA series and (e) AC-GA series. Standard patterns of Fe₃O₄ (04-009-8428), Fe (04-014-0264) and Fe (04-004-2475) matched by Panalytical HighScore Plus software with built-in ICDD database were present along as purple, blue and green lines, respectively. Activated carbon (AC-X-Y) from hydrothermally carbonized glucose or glucosamine with and without iron (X: G, GA, GFe, or GAFe) prepared at temperatures of Y: 800 °C for 4 h.

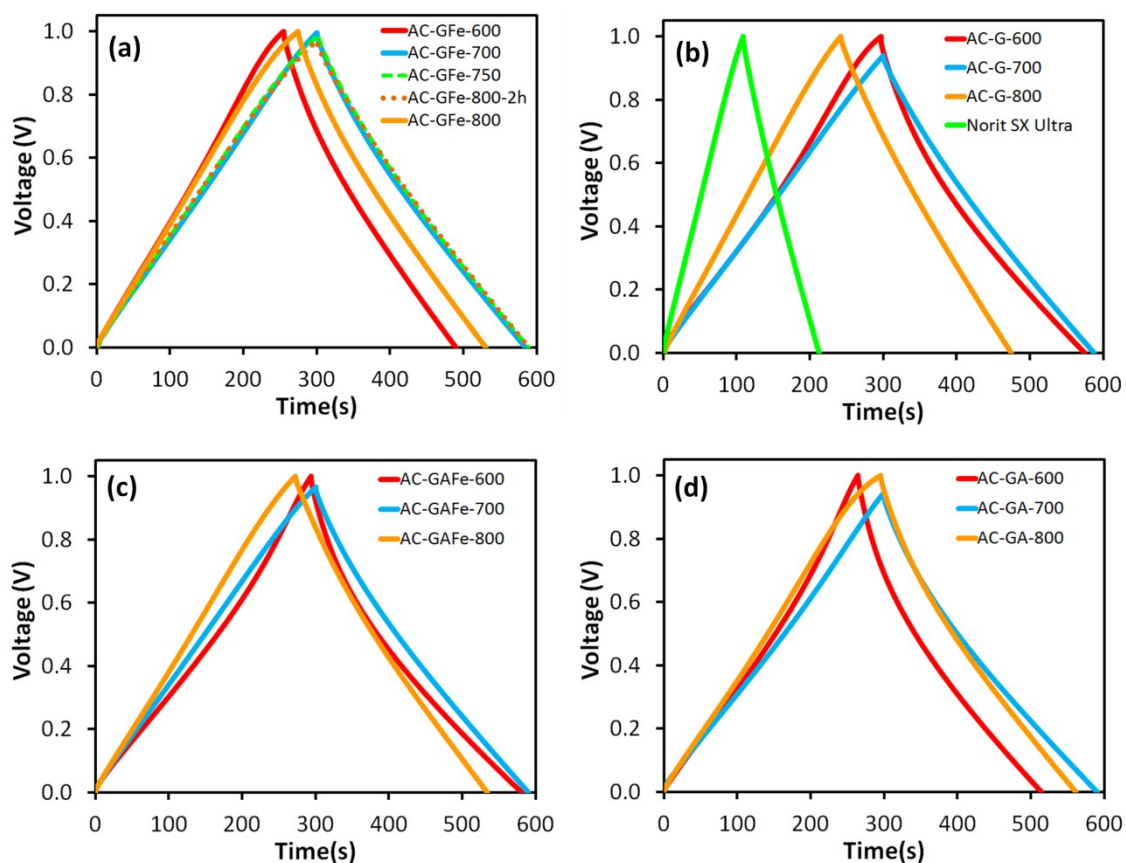


Figure S10. Galvanostatic charge-discharge curves of different AC series at 0.2 A/g. Activated carbon (AC-X-Y) from hydrothermally carbonized glucose with and without iron (X: G, GA, GFe, or GAFe) prepared at temperatures of Y: 600-800 °C for 4 h (except 2 h for AC-GFe-800-2h).

Note: Several curves charged to (and subsequently discharged from) upper voltage limits less than 1 V due to the time limit of 300 s set for the chronopotentiometry. However these have negligible effect on the derived specific capacitances.

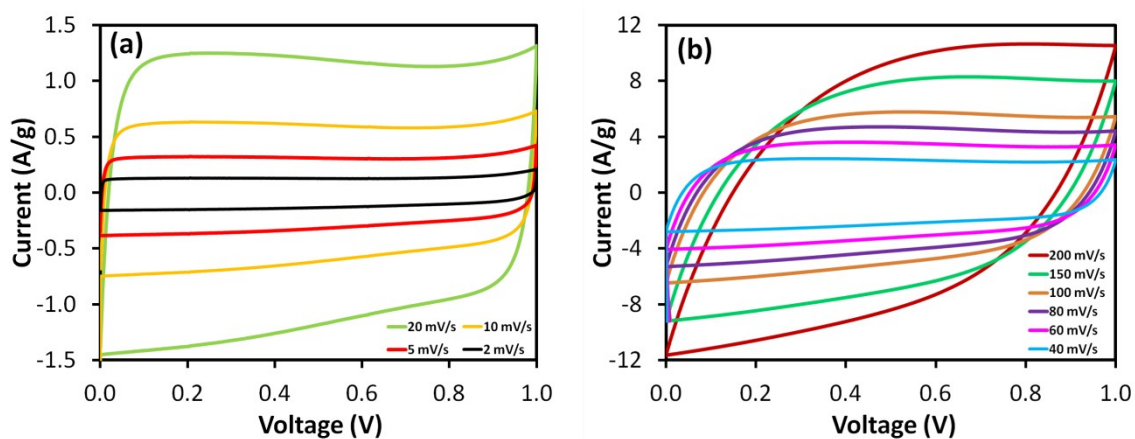


Figure S11. CV curves of sample AC-G-700 at different scan rates from 2 to 200 mV/s.

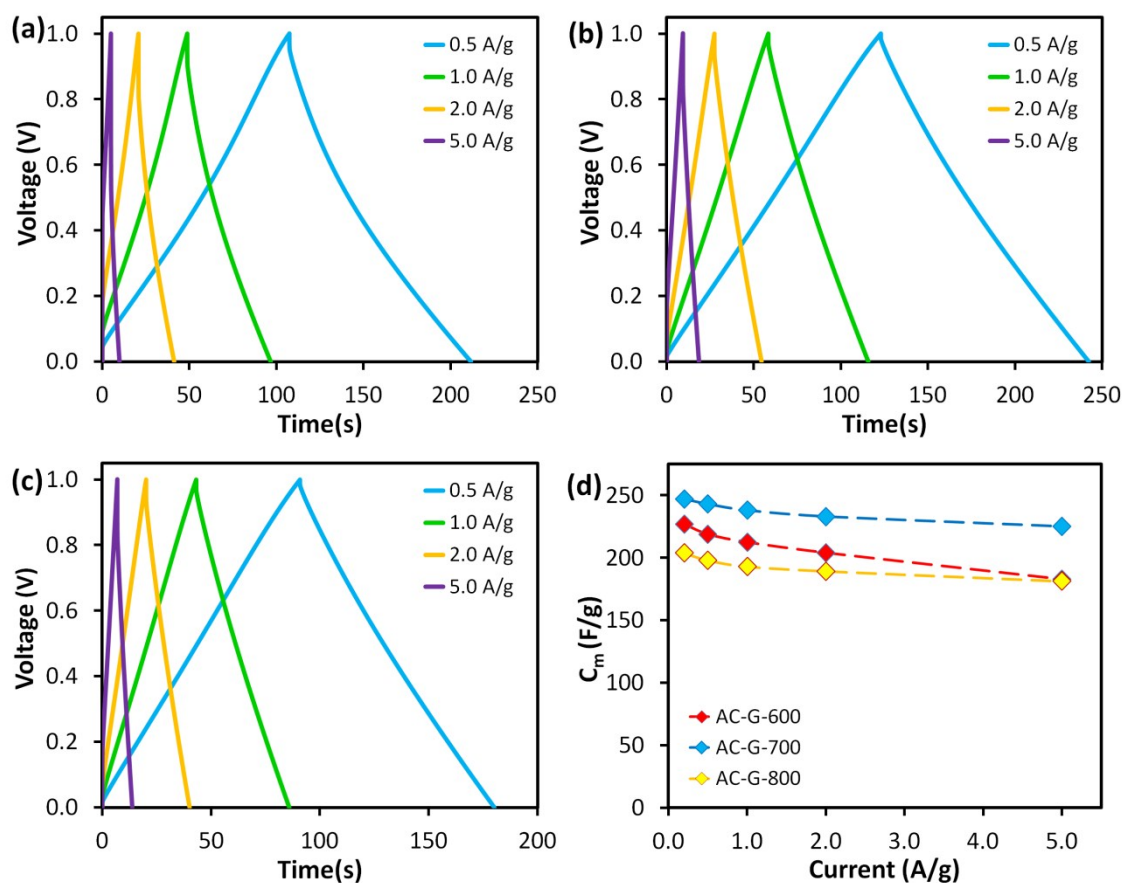


Figure S12. Galvanostatic charge-discharge curves of AC-G series: (a) AC-G-600, (b) AC-G-700, (c) AC-G-800; and (d) corresponding specific capacitances (C_m) calculated from the discharge curves.

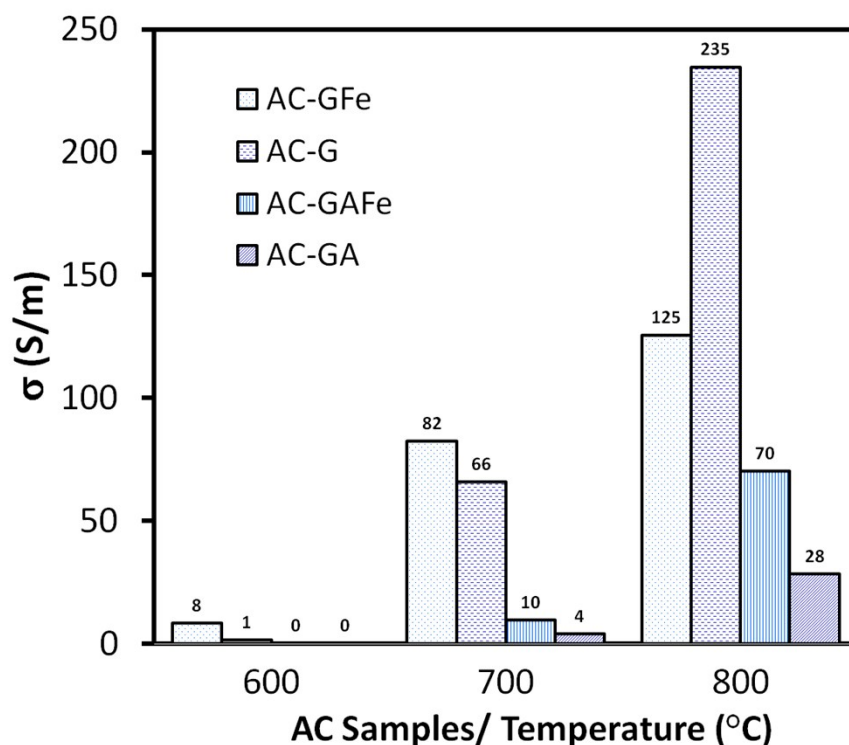


Figure S13. Effects of activation temperatures and precursor types on electrical conductivity of AC powders pressed at 7 MPa. Activated carbon (AC-X-Y) from hydrothermally carbonized glucose or glucosamine with and without iron (X: G, GA, GFe, or GAFe) at 600-800 °C for 4 h. Apart from the chart, the electrical conductivities of AC-GFe-750, Norit SX Ultra and carbon black are 100, 198 and 411 S/m, respectively.

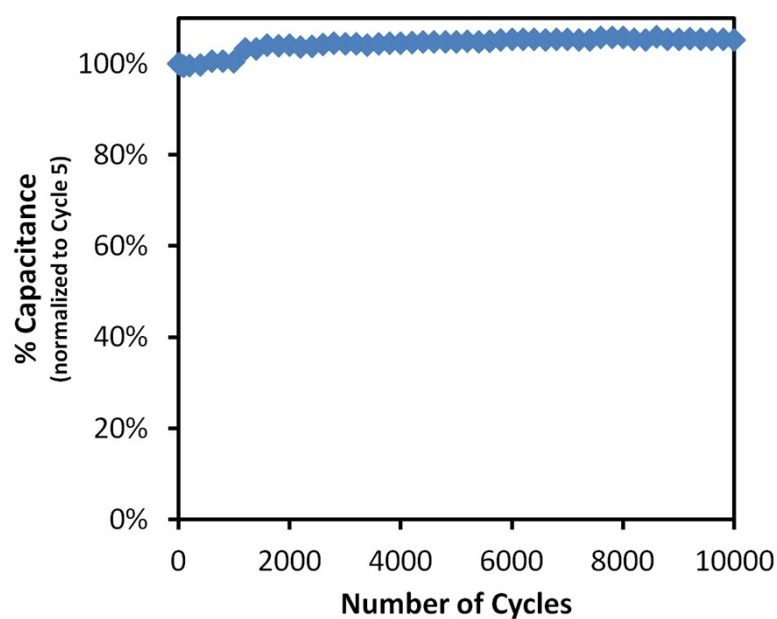


Figure S14. Cycling life time of AC-G-700 at scan rate of 100 mV/s in 6 M KOH.

Raman studies are performed with a laser wavelength at 532 nm and presented in Figure S14. For all samples, two broad bands typically associated with disordered amorphous carbon materials can be observed in the wavenumber between 1200 to 1800 cm^{-1} : the G-band ("graphitic") centred at 1570-1590 cm^{-1} and the D-band (disorder-induced) centred at 1350-1370 cm^{-1} . However, no further information on the extent of graphitization can be obtained on ACs prepared at different temperatures (e.g. AC-G series), due to the similar intensity of G-band.

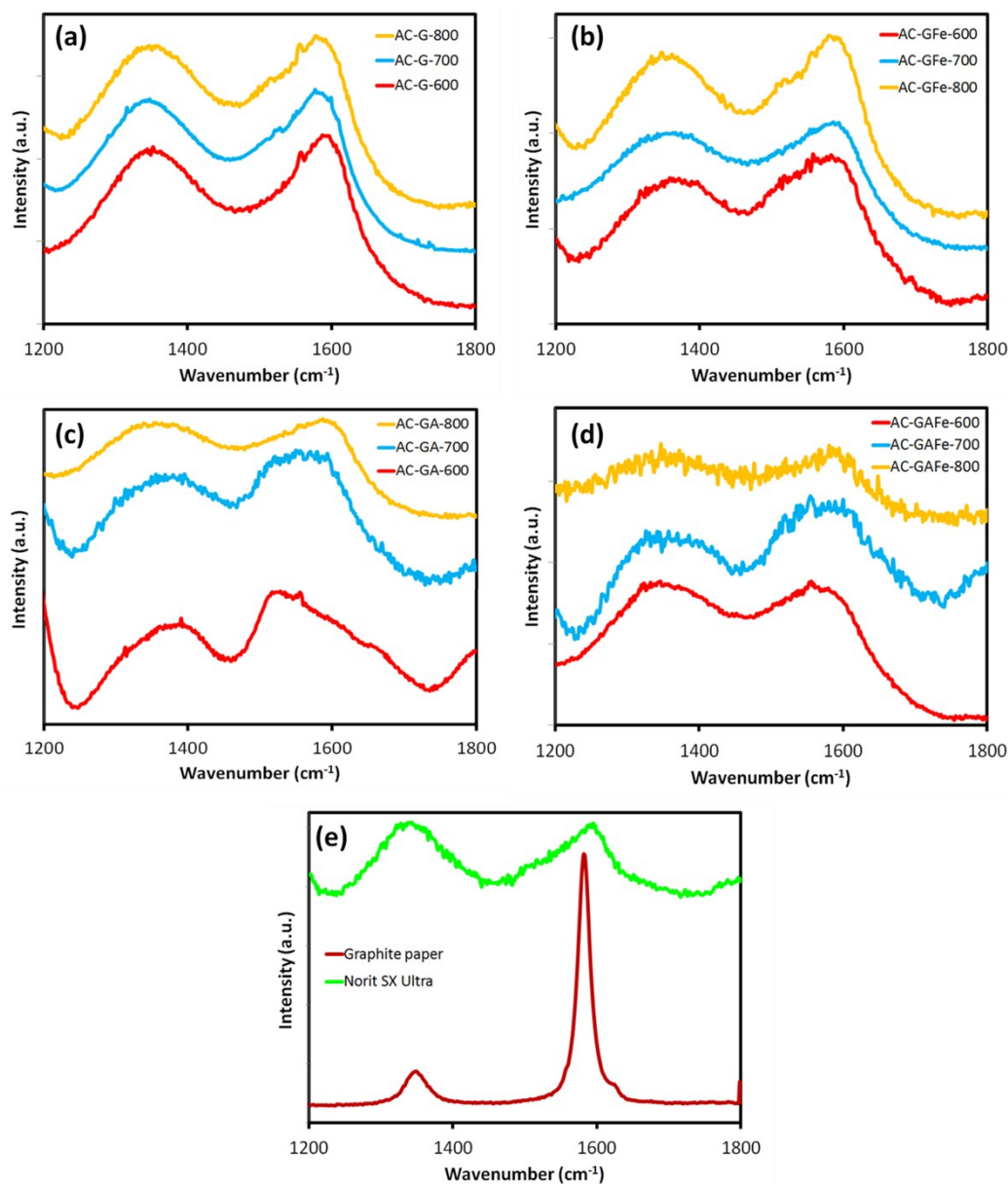


Figure S15. Raman spectra of AC samples and references recorded at a laser wavelength of 532 nm. Activated carbon (AC-X-Y) from hydrothermally carbonized glucose with and without iron (X: G, GA, GFe, or GAFe) prepared at temperatures of Y: 600-800 °C for 4 h (except 2 h for AC-GFe-800-2h). Norit SX Ultra and graphite paper are used as references.

The morphology and microstructure of the AC-G-700 sample was examined by SEM and TEM. The typical SEM image displayed in Figure S16a is similar to all samples. The carbon particles possess irregular alveoli shapes, with various conchoidal cavities and smooth surface. The TEM image in Figure S16b shows a separate part of the carbon particle and it was used for further examinations. As presented in the High-resolution TEM (HRTEM) image in Figure S16c the porosity of the activated carbon is made up of randomly distributed micropores with irregular sizes. Also, some graphitic domains at the edge of the sample are clearly observed (a boxed area is enlarged in the inset). The high-angle annular dark-field (HAADF)-STEM images presents the highly porous structure and thus the “fluffiness” of the sample.

Electron energy loss spectroscopy (EELS) was applied to further investigate the sample. Figure S17 is the EELS spectra of AC-G-700 and amorphous carbon. The latter is as a reference sample, in which graphite is absence. The intensity of the two EELS spectra is normalized. It is clearly seen that the spectrum of AC-G-700 has a higher ratio for the π^* peak to the σ^* peak (0.53) than of amorphous carbon (0.4). The increase of the π^* peak is the evidence of graphitic structure presence in AC-G-700.

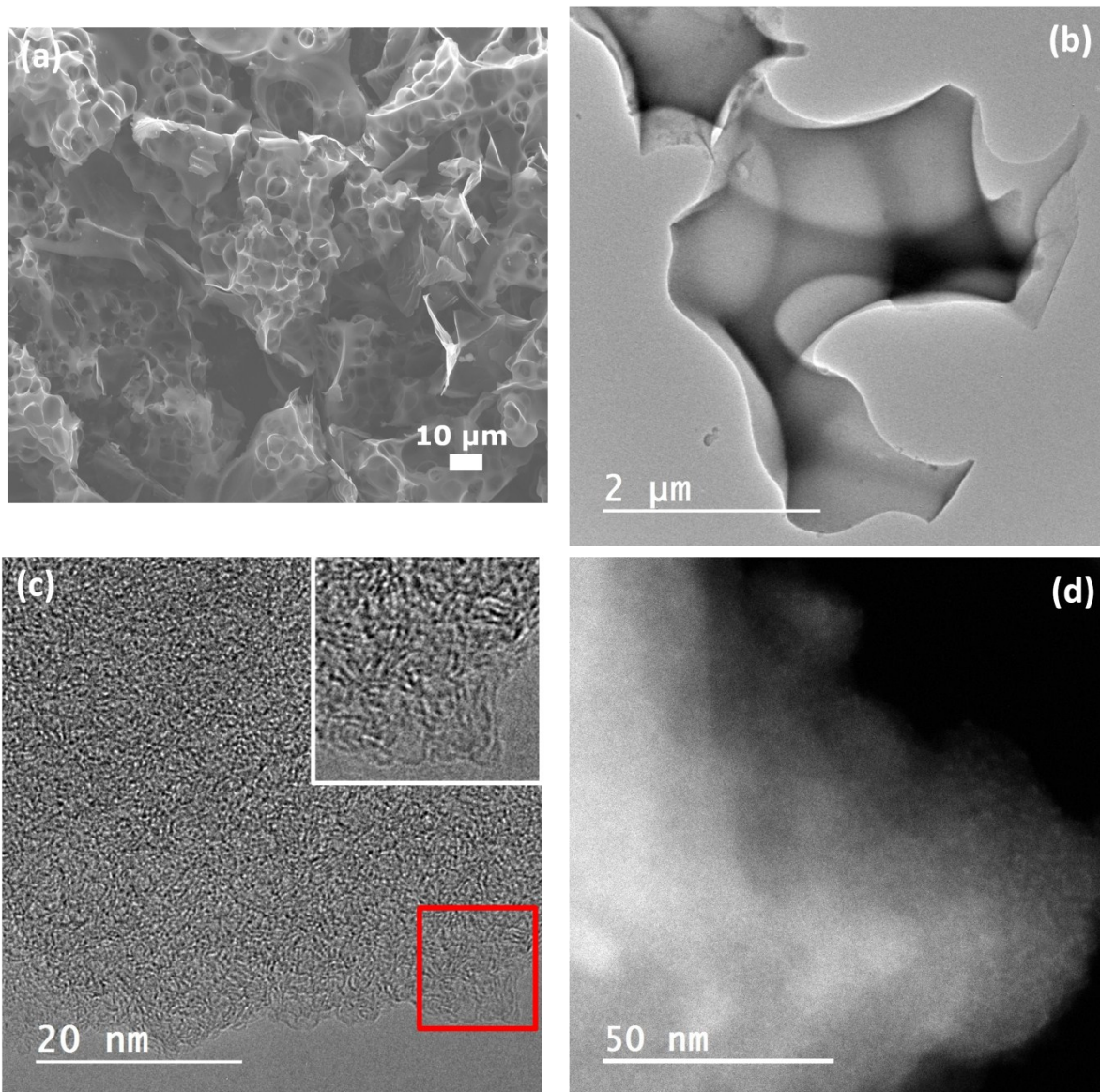


Figure S16. (a) SEM and (b) BF-TEM images showing the general morphology of sample AC-G-700 at low-magnification. (c) HRTEM and (d) HAADF-STEM images revealing the presence of graphitic layers and porous structures in the sample.

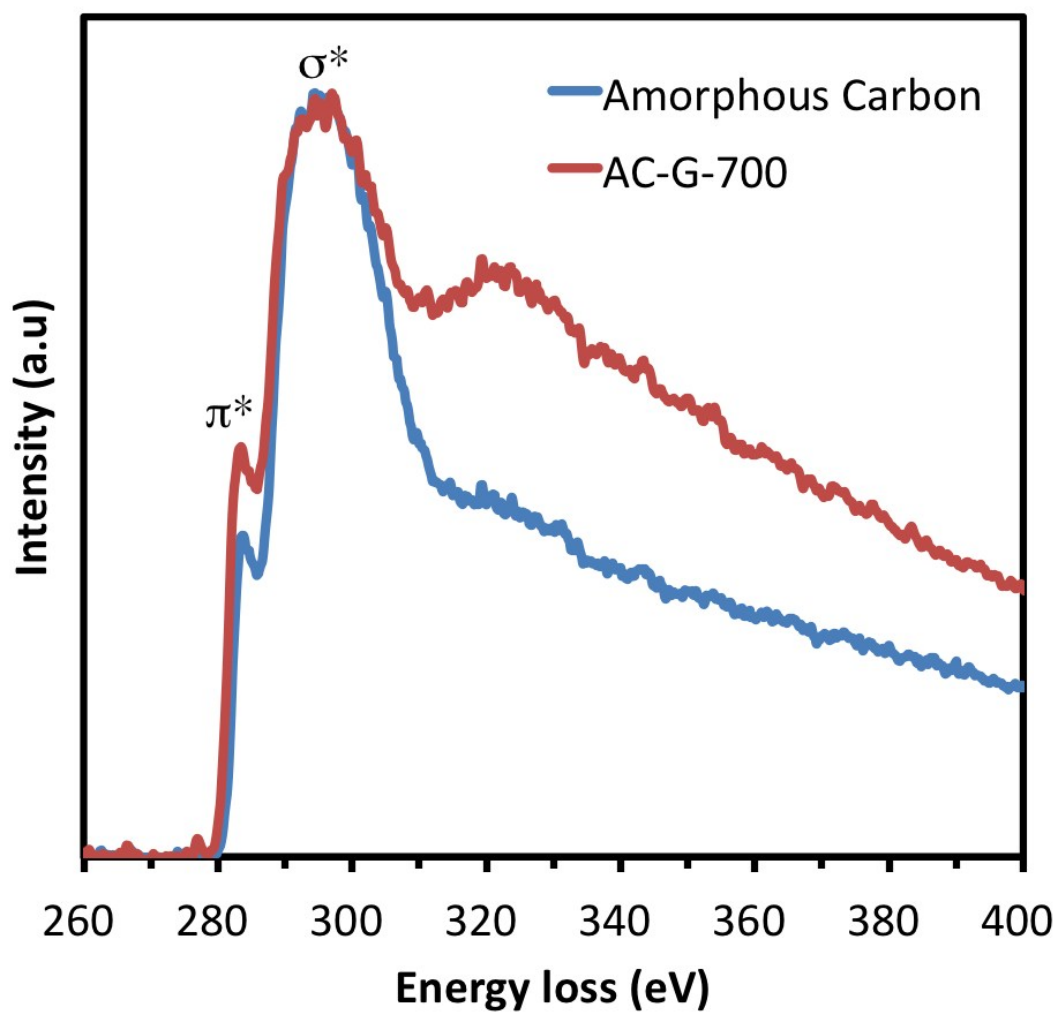


Figure S17. EELS spectra in the carbon K-edge region from the sample AC-G-700 and amorphous carbon.